JOURNAL OF MATERIALS SCIENCE 7 (1972) 1037–1051

Flow-stress recovery of nickel-aluminium alloys

T. V. NORDSTROM
Sandia Laboratories, Albuquerque, New Mexico

C. R. BARRETT
Department of Materials Science and Engineering, Stanford University, Stanford, California, USA

Flow-stress recovery measurements along with structural observations using electron microscopy have been carried out on room-temperature prestrained alloys of Ni-11.9, 13.1 and 13.5 at.% Al aged at 735°C. These alloys contained respectively 0, 5, and 8 vol% γ' (Ni_3Al) in a fine dispersion. Samples were recovered at and below the ageing temperature for times ranging from 0.1 to 100 h. The influence of volume fraction of γ', γ' distribution, amount of prestrain and recovery temperature on recovery kinetics was investigated.

Results for samples recovered at 735°C showed a large fractional recovery (about 30%) following the first 0.1 h anneal for all samples. About 50 to 70% of the flow stress is recovered at the end of 100 h recovery anneals. The changes in dislocation structure agreed quantitatively with the changes in flow stress.

Interpretation of the data in terms of a network growth model of recovery show the solid solution alloy to agree with theory for long recovery times ($t > 10$ h) whereas the γ'-strengthened alloys deviate considerably from the simple model.

1. Introduction

Although considerable work [1-3] has been carried out studying the recovery of cold-worked metals and alloys, relatively little emphasis has been placed on parallel studies of the recovery of physical properties and the concurrent changes in dislocation substructure. This is especially true of studies on flow-stress recovery in both single-phase alloys and precipitation- or dispersion-hardened systems. Previous investigations have established the nature of the important recovery mechanisms but there has been little attempt to quantify these observations and relate then to existing theory.

The processes involved in recovery can be divided into the following three distinct groups on the basis of the relative size or distances involved in their occurrence:

1. Short range mechanisms such as annihilation of dislocation loops and dipoles [4], rearrangement of dislocations in tangles [5, 6] and, in the case of two-phase materials, reaction of the dislocation tangles around the precipitates at the interface between matrix and particles [7]. These processes may be controlled either by glide or climb of dislocations.
2. Medium range mechanisms such as three-dimensional network growth under dislocation-climb control [8].
3. Long-range mechanisms such as enlargement of the average cell size by subgrain coalescence [9].

All of these mechanisms have received some study and have been treated mathematically in various recovery models.

In the present study, interest centres primarily around the mechanism of growth of a three-dimensional dislocation network by climb. This area is of special interest because measured changes in the flow stress can be compared with the predicted recovery kinetics of the model of network growth as first proposed by Friedel [10]. Quantitative measurements of the change in the dislocation density can be made and related to the flow-stress changes directly. Study of this mechanism is important to high-temperature

creep models where the rate-controlling mechanism is often related to the climb-controlled motion of dislocations [11].

In considering the role that a second phase plays in recovery, it appears likely that if network growth is the controlling mechanism, then the presence of the second phase inhibits the process if the spacing of the dislocations is of the order of or greater than the particle spacing. A second phase should also restrict the motion of cell walls if recovery occurs by enlargement of the cell size as has been proposed for the TD-nickel system [12].

The Ni-Al system was chosen for this study for the following reasons:

1. Suitable composition and heat-treatment yields either a solid solution or uniform distribution of the coherent, cube-shaped γ' (Ni_3Al) precipitate. The precipitate structure is known to coarsen slowly [13] and thus assures a stable precipitate structure during recovery.
2. The distribution of γ' can be controlled so that the uniform distribution of interparticle dislocations desired for quantitative dislocation density studies can be obtained.
3. The system has great technological importance since it is known that γ' is the principal high-temperature strengthening mechanism in many commercial nickel-base alloys [14].

Thus the influence of a second phase on recovery along with variables such as amount of prestrain and recovery temperature could be studied by using this alloy system.

2. Experimental Procedure

The three alloys used in this investigation were supplied by the International Nickel Company in the form of bars 2.5 × 2.5 cm cross-section. They had been prepared by vacuum induction-melting, cast into a 10 × 10 cm ingot and hot-worked at 1150°C to the as-received form. The detailed chemical analysis of the three alloys is given in Table I. The equilibrium structures of the three alloys, as predicted by the phase diagram for 735°C, which was the ageing-temperature for most of the tests, are as follows: alloy SS (11.9% Al) is a solid solution of Al in Ni, alloy LP (13.1% Al) is an alloy with a low precipitate content, with about the same matrix composition as alloy SS and about 5 vol% γ', and alloy MP (13.5% Al) is an alloy of medium precipitate content that contains about 8 vol% γ'.

The bar stock was rolled at 25°C to a thickness of 1 cm, annealed 0.5 h at 1200°C and rolled again at 25°C to a thickness of 0.05 cm. All annealing and recovery treatments were carried out in an atmosphere of dry nitrogen with temperature control of ± 2°C. Tensile samples were machined from the sheet with a gauge section width of 1 cm and length of 2.5 cm with the tensile axis parallel to the rolling direction.

Fig. 1 is a schematic diagram of the thermal and mechanical treatment of the machined samples. The thermal treatment consists of solution-treating at 1050°C for 0.5 h, water-quenching, ageing at various temperatures to obtain a stable structure and water-quenching. Following ageing, a given amount of tensile strain was introduced at 25°C. This was followed by recovery anneals for times ranging from 0.1 to 100 h. In most instances, the recovery temperature was identical to the ageing temperature. A second tensile test was then run on the samples at room-temperature to determine the extent of flow-stress recovery.

The flow-stress parameters measured are also shown in Fig. 1. They are σ_{y^1}, the 0.2% offset yield strength of the as-aged samples; σ_{u^1}, the flow stress at the end of the prestrain cycle (also the yield stress for unrecovered samples); and σ_{y^2}, the 0.2% offset yield strength for the tensile test following recovery. The degree of flow stress recovery is evaluated in two ways. It is presented as the recovery parameter, R, where

$$R = \frac{\sigma_{u^1} - \sigma_{y^2}}{\sigma_{u^1} - \sigma_{y^1}} \quad (1)$$

This is the fractional decrease in the flow stress following the recovery anneal: zero indicates no

TABLE I Detailed composition of alloys used in studies

	at. %	wt %							
	Al	Al	C	S	Co	Mn	Si	Cu	Ni
SS	11.9	5.85	0.003	< 0.001	< 0.01	< 0.01	0.013	0.012	Bal.
LP	13.1	6.50	0.004	< 0.001	< 0.01	< 0.01	0.013	0.013	Bal.
MP	13.5	6.68	0.023	< 0.001	< 0.003	< 0.004		0.005	Bal.

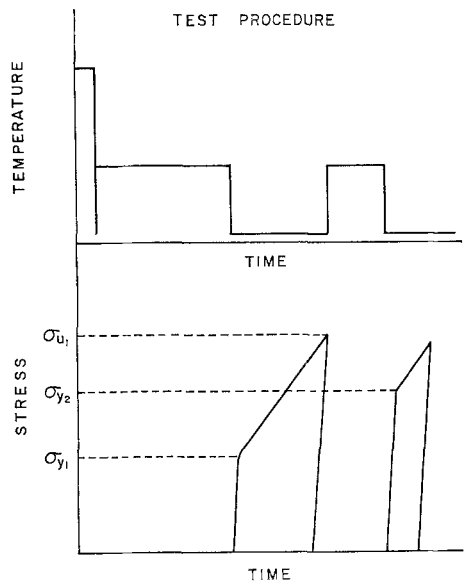

Figure 1 Schematic of ageing and testing sequence used.

recovery and unity indicates complete recovery. This representation is useful because it decreases the scatter due to variation in yield stress from sample to sample. The physical interpretation of the results is difficult, however, when comparing samples with large differences in work-hardening or when relating to recovery models.

The second method used involves a measure of the internal stress or the strain-hardening component of the flow stress given by

$$\sigma_i = \sigma_{y^2} - \sigma_{y^1} . \quad (2)$$

σ_i is that portion of the yield stress that is due to effects other than the inherent strength of the annealed material as given by σ_{y_1}. Thus σ_i should be a measure of the hardening due to dislocation-dislocation or dislocation-particle interactions. When comparing results with theoretical models of recovery, σ_i is the variable most convenient to consider [10].

2.1. Effects Studied

2.1.1. Volume fraction of precipitate

Following solution-treatment at 1050°C for 0.5 h and quenching, samples of the three alloys were aged 200 h at 735° C. 735° C was chosen because electron microscopy studies showed that the as-deformed state of alloy MP had a uniform distribution of interparticle dislocations. Samples were then deformed to 10% true tensile strain at room temperature. Following prestraining, specimens were recovered at 735°C for 0.1, 1, 10, 50 and 100 h, water-quenched and retested at room-temperature. The strain-rate used in all tests was 0.01 min^{-1}. The heat-up time for a sample in the recovery anneals was 2.5 min and allowance was made for this during the 0.1 h recovery tests by actually having the sample in the furnace for 8.5 min.

2.1.2. Precipitation distribution and recovery temperature

These two properties are interrelated since the ageing and consequently the recovery temperature controls the precipitate distribution. Alloy MP was aged 200 h at 650, 700, and 735°C following the solution-anneal. Samples were strained 10% at room temperature and recovery tests were performed at the various ageing temperatures for times of 0.1 to 100 h.

2.1.3. Strain

True strains of 5, 10, and 20% were used with alloys SS and MP following ageing at 735°C to study the effect of amount of prestrain, or more correctly the amount of work hardening, $(\sigma_{u^1} - \sigma_{y^1})$, on recovery. Recovery tests were carried out at 735°C for times ranging from 0.1 to 100 h.

2.1.4. Temperature of recovery anneal

This variable was studied in alloy MP by recovering samples 1 h at temperatures from 250°C up to 735°C in about 100-degree increments following 10% deformation at room-temperature. Recovery temperature effects were also studied in alloy SS by recovering a full series of samples at 650°C in addition to the tests performed at 735°C.

2.1.5. Electron microscopy

Samples were examined in the as-aged, as-strained and as-recovered condition for the majority of the tests described above. To prepare the samples, the gauge length of the sample was cut out, the oxide layer removed by lapping with 240 grit paper and the resulting 2 × 1 × 0.04 cm sheet was electro-thinned in 80% methanol/20% sulphuric acid at 10°C operating at 36 V, 10 A until the sheet was about 0.015 cm thick. 0.3 cm discs were then trepanned out of the central gauge portion via spark-machining, and final electro-thinning was done in 90% ethanol/10% perchloric acid at 0°C in a Fischione jet-polisher. Samples were examined at 100 kV in a Philips EM 200 equipped with beam-tilting coils for

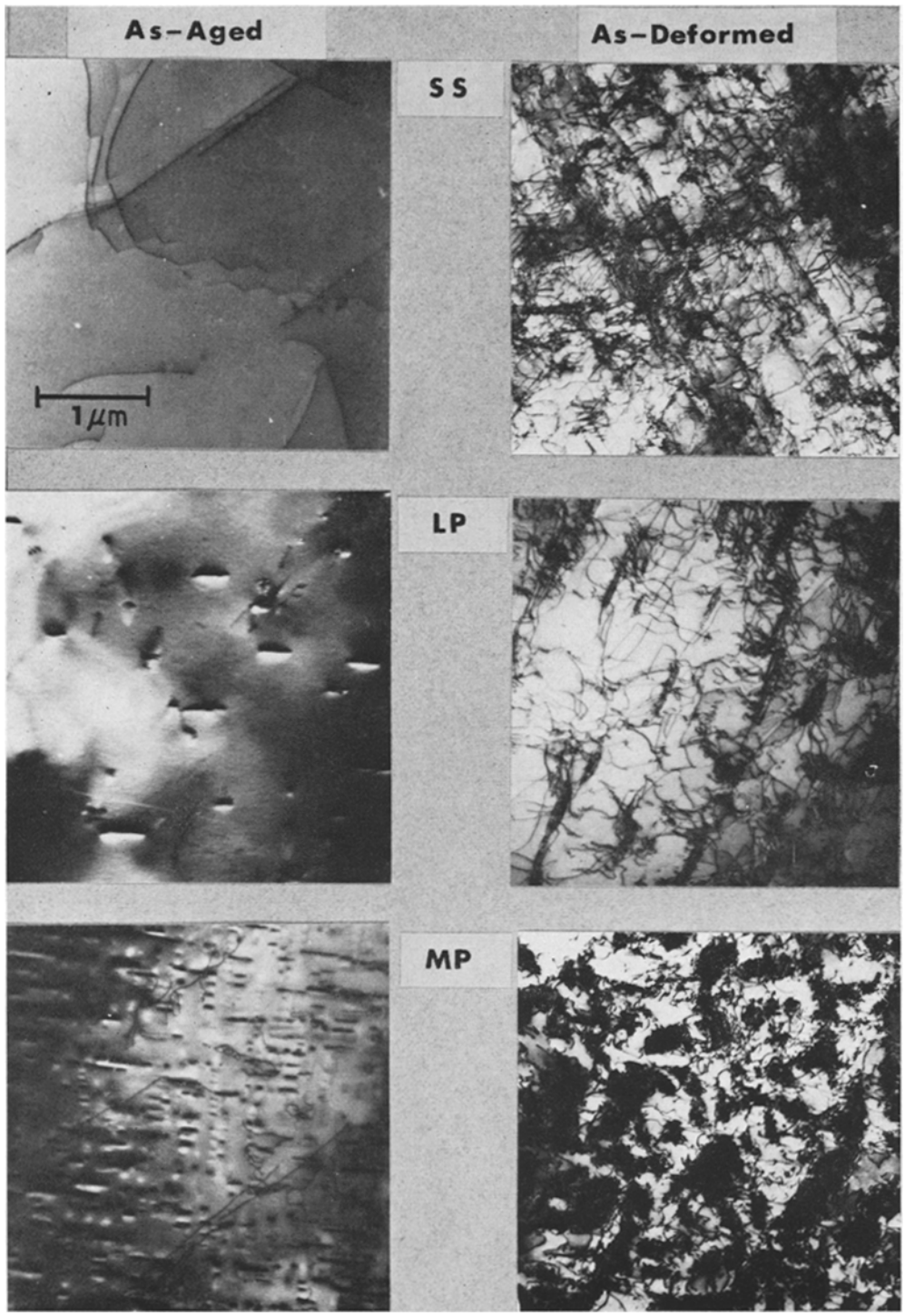

Figure 2 Substructure changes in each alloy for as-aged and as-deformed state. Aged 200 h at 735°C, $\epsilon = 10\%$.

dark-field work. Dislocation density counts were made using the random line intersection method of Smith and Guttman [15] assuming a foil thickness of 2000 Å. At least forty different areas were counted for each value reported.

3. Results

The results are presented in sections as outlined in the experimental procedures.

3.1. Alloy Effects

Fig. 2 shows the microstructure of the three alloys in the as-aged and as-deformed conditions. In the as-aged state, the three alloys have a dislocation density of about 10^6 to 10^7 cm^{-2}. For alloy MP, the average precipitate size is about 1000 Å and the cubic particles cluster slightly along the $\langle 100 \rangle$ directions. Calculations of an average particle spacing on the $\{111\}$ planes gives a value of about 2000 Å. This spacing is of the order of the average dislocation segment length in the as-deformed state (10% strain) calculated from the measured interparticle dislocation density (about 1100 Å) and thus allows a good comparison with the suggestion that the particles will inhibit the recovery process for this case. Alloy LP exhibits considerable inhomogeneity in the observed volume fraction of γ' and concurrently in the as-annealed yield strength. This is probably due to inhomogeneity in the Al content. Samples having γ' in the amount shown in Fig. 2 and with equal values of σ_{y_1} were used in all the studies reported here. The average γ' particle size is again about 1000 Å with a spacing of about 1 μm. The grain size for the three alloys was found to be about 0.01 cm. A uniform ring pattern was obtained for Laue back-reflection studies suggesting that no strong texture was present in the as-aged material.

The as-deformed structures of the solid solution (alloy SS) has diffuse slip-bands typical of room-temperature deformation for moderate stacking fault energy metals. Alloy LP also has a band type deformation structure. In addition, there is also evidence of dislocation interacting with the γ' particles with some formation of dislocation nests around the particles. Observations in alloy LP have shown clear evidence of particle shearing with obvious offsets in individual particles that lie along slip bands although the offsets are not of the magnitude seen by other investigators in similar systems [16]. The orientation of the slip bands corresponds to slip on the $\{111\}$ planes.

Alloy MP shows a much more uniform type of deformation. Each of the γ' particles is surrounded by a nest of dislocation loops and debris left by dislocations bowing around the particles. There is also a uniform distribution of interparticle dislocations and other debris in the interparticle region. Because of the extent of deformation, there are few obvious examples of dislocation pairs as has been reported previously in the literature [17]. Superlattice observations showed no evidence of massive shearing of particles on single slip planes as seen in alloy LP. The γ' particles in alloy MP did show some contrast effects that differed from the annealed state. There were line contrast effects that appeared to be at the γ'-matrix interface and lay in directions corresponding to the $\{111\}$ planes and thus were probably associated with some slight shearing of the particles. Values for the measured dislocation density, ρ, for alloys SS and MP in the as-deformed state are given in Table II. In determining ρ for MP, only interparticle dislocations were counted. Those dislocations in the nests around the particles in the as-deformed state were not counted because individual dislocations could not be clearly resolved.

TABLE II Dislocation densities for alloys SS and MP prestrained 10% and recovered at 735°C
ρ = values $\times 10^9$ cm^{-2}

Alloy	Recovery time (hours)					Standard
symbol	0	0.1	1	10	100	deviation
SS	12	9	7	6	5	± 1.7
MP	25	17	17	15	13	± 2

Fig. 3 shows the variation of recovery parameter and σ_i with recovery time for the three alloys. Also on the graph are average values of the yield strength and amount of work hardening σ_{wh} given by $\sigma_{wh} = \sigma_{u_1} - \sigma_{y_1}$. Specific values of yield strengths were used for the calculation on each individual test rather than the average values.

A significant feature of the recovery parameter results is the large fractional recovery (about 30%) during the first 0.1 h. Similar studies on high purity aluminium [4] show a large fractional flow-stress recovery in the first 0.1 h. This large change during the first 0.1 h is probably related to the rearrangement of dislocations in tangles and the annealing out of small dislocation defects such as loops and dipoles which are classified as

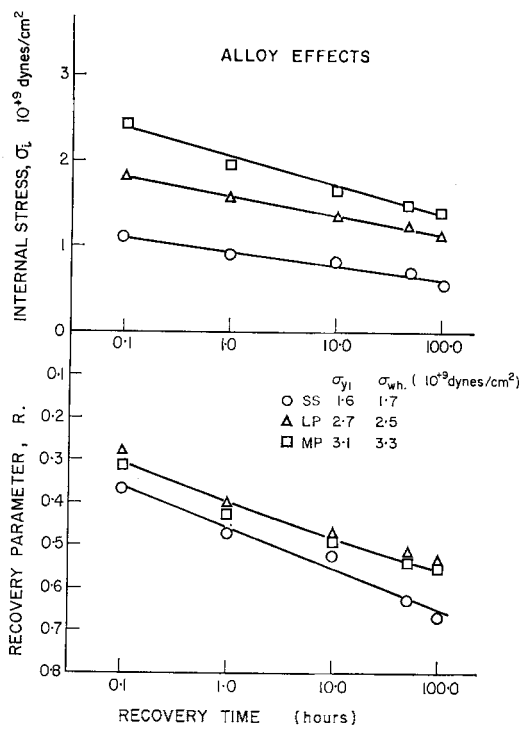

Figure 3 Variation of recovery parameter and internal stress for three alloys aged 200 h at 735°C, $\epsilon = 0.10$, recovered at 735°C.

short range recovery processes. Preliminary experiments showed that practically all of this initial recovery occurred on heating to the recovery temperature. Because of the rapid nature of this process relative to the heat-up time ($\sim$ 2.5 min), it was not possible to measure an activation energy for the process and positively identify the rate-controlling mechanisms.

The solid solution recovers a larger fraction during the initial 0.1 h and continues to recover at a slightly higher rate than the two alloys with γ'. The long-time tests have been corrected for any concurrent age-softening of the materials by ageing undeformed samples an additional 100 h and then measuring the flow stress. This correction was zero for SS and was about 0.05 on the fractional recovery for alloys LP and MP. Although it can be argued that the ageing characteristics may be influenced by plastic deformation it was found that there was no measurable difference in γ' particle size for undeformed and deformed (10% strain) samples after ageing the additional 100 h.

In general, the data can be represented fairly well by the expression

$$R = A - B \ln (t) \qquad (3)$$

Other observers have found that expressions of the same form fit their results [18, 19] but no models are available which explain such a result. There is a slight deviation from this result for LP and MP at the longest times with the rate of recovery being somewhat less than that given by Equation 3. Previous work has shown essentially the same effect on an approach towards a constant fraction of recovery as time progresses [4, 20]. This would be expected since the driving force for the recovery process is continually being decreased as the process continues. A more detailed analysis of the recovery rate will be given in the discussion.

The rate of decrease of σ_i with time varies directly with increasing aluminium content for the three alloys. This is consistent with the fact that the initial work-hardening, σ_{wh}, also varies in the same way so that the driving force for recovery is increased at high aluminium contents. The results again show an approximate linear relation with log of time. Data of this type from other recovery studies are not available for comparison. In the discussion section, we will cover the comparison of the observed variation in σ_i with that predicted by theory.

Fig. 4 shows a series of electron micrographs illustrating representative structures for the recovery of alloy SS at 735°C for times up to 100 h. These micrographs plus the dislocation density measurements listed in Table II illustrate the changes in structure accompanying recovery. After 0.1 h, the changes are the disappearance of the small loops and debris and the breakdown of the slip bands. The small loops and dipoles would be expected to disappear at a rapid rate due to the short distances of diffusion involved and the fact that there is generally detected to be an excess of vacancies in an as-deformed metal [21] and thus these can act to aid in the recovery processes during short times. Close examination of the slip bands shows that some fine two-dimensional networks are beginning to form in the slip-band regions. There is also a measurable decrease in the dislocation density. After 1 h of recovery, the slip bands have essentially disappeared and there are now two-dimensional networks plus a uniform distribution of well defined dislocations between sub-boundary networks. Again a decrease in the overall density of dislocations was found. Continued recovery

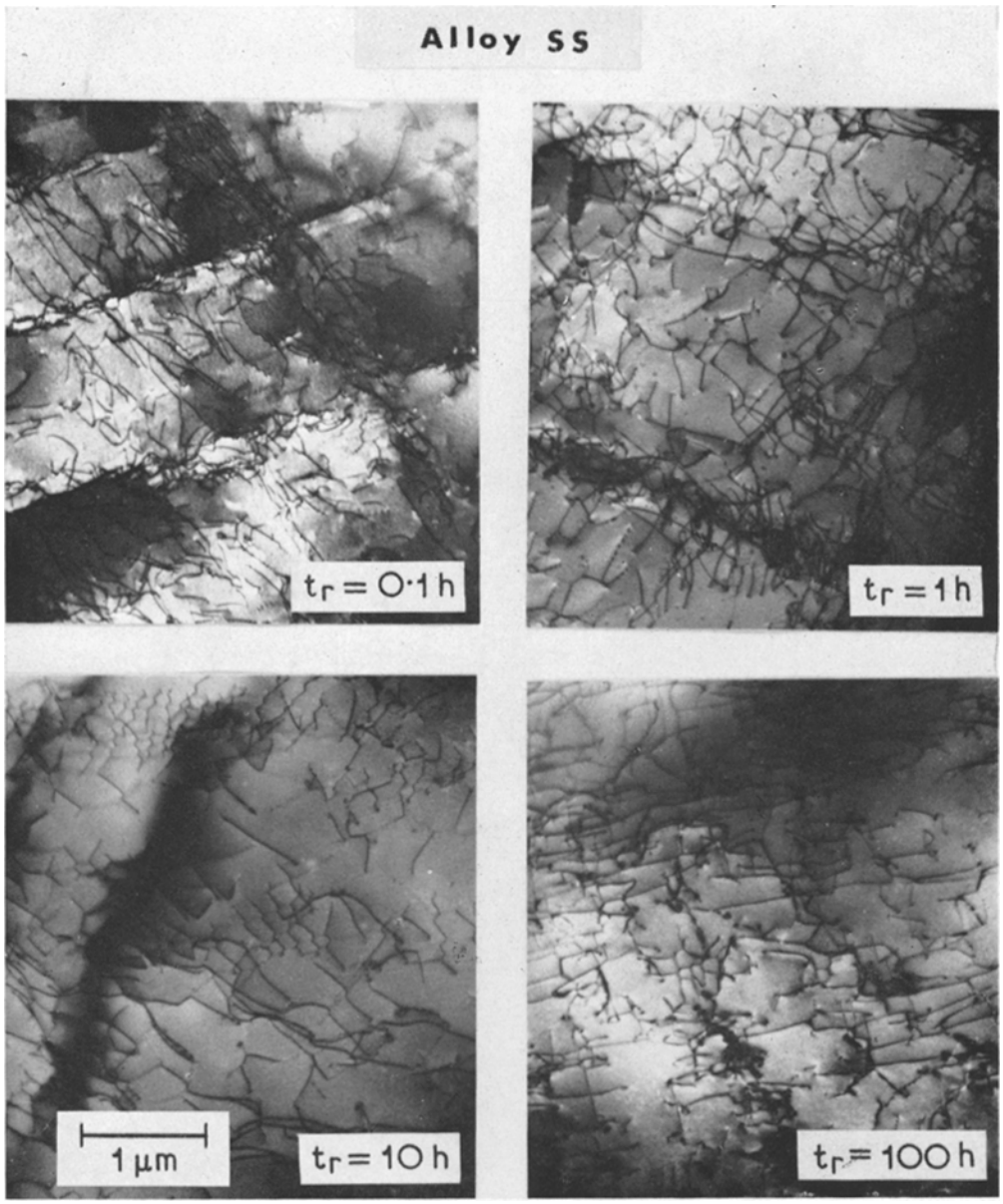

Figure 4 Variation of dislocation structure in alloy SS for various times of recovery at 735° C, following 10% strain.

TABLE III Precipitation distribution and recovery temperature data for alloy MP

Ageing and recovery temperature (° C)	Particle size (Å)	Particle spacing (Å)	σ_{y1} 10^9 dyn cm^{-2}	σ_{wh} ($\epsilon = 0.10$) 10^9 dyn cm^{-2}	Recovery parameter for various times (h)			
					0.1	1.0	10	100
650	400	1000	3.6	2.8	0.27	0.32	0.38	0.50
700	700	1500	3.3	2.9	0.31	0.34	0.41	0.46
735	1000	2000	3.1	3.3	0.31	0.43	0.49	0.55

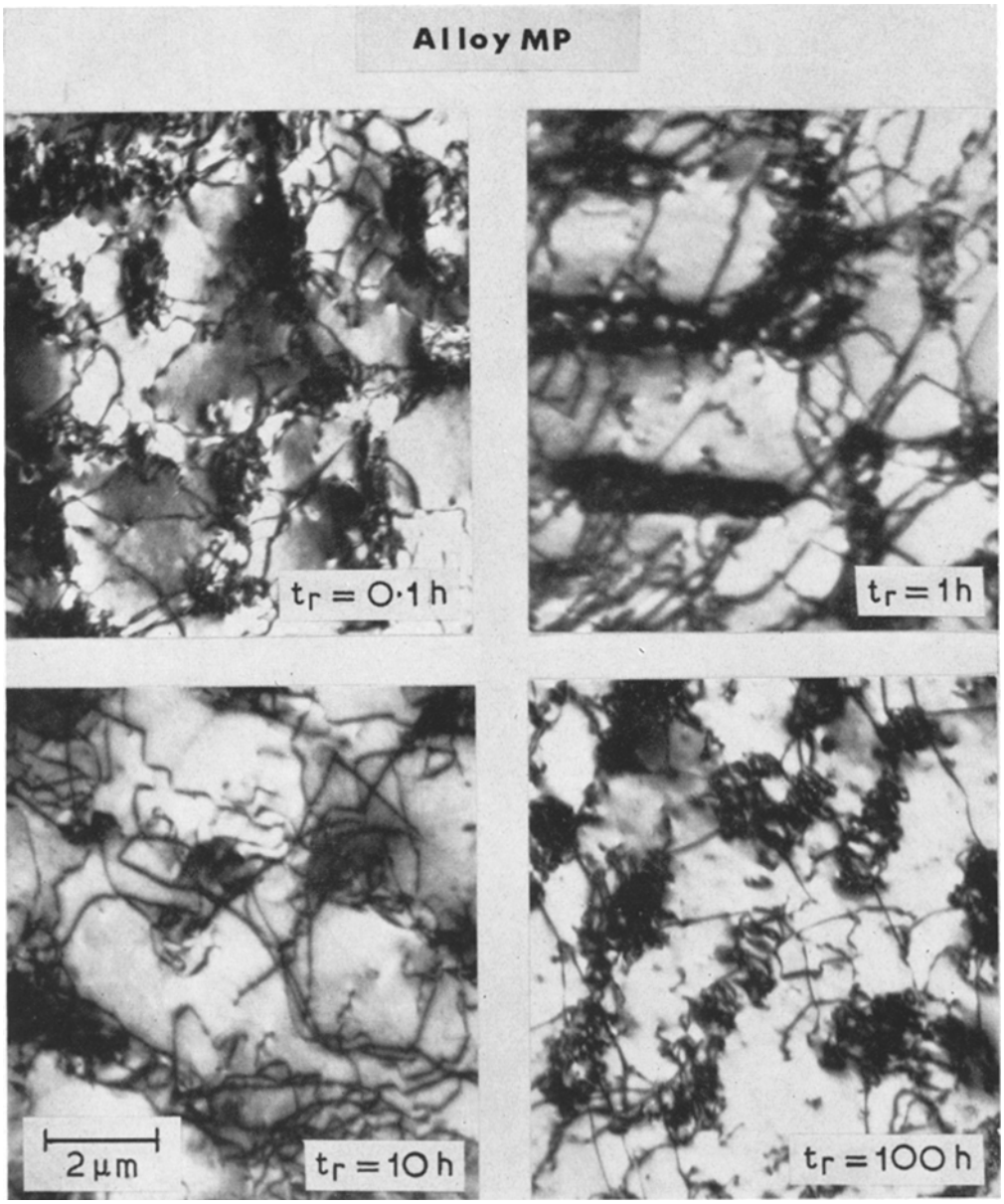

Figure 5 Variation of dislocation and γ' particle structure for alloy MP after various recovery times at 735°C, following 10% strain.

results in further decrease in the overall density of dislocations and an increase in the perfection of the two-dimensional dislocation networks. At the end of the 100-h recovery, alloy SS begins to show evidence of a well-defined cell structure.

Fig. 5 is another series of electron micrographs showing the substructural variations seen in alloy MP following the various recovery anneals. Parallel interparticle dislocation density measurements are presented in Table II. The initial changes are the elimination of small loops and other fine debris scattered in the matrix, plus a significant change in the nature of the dislocation structure around the individual γ' particles. Many of the dislocations that formerly surrounded the particles have either been

annihilated or have taken up positions as interface dislocations at the matrix-γ' interface. These dislocations can act to accommodate the approximately + 0.5% lattice misfit between the precipitates and the matrix. A simple calculation shows that the spacing of dislocations needed to accommodate this coherency strain is one dislocation every 350 Å with the dislocations arranged in a square array. This would mean that the average precipitate cluster should have about ten interface dislocations along its length to fully accommodate the mismatch. The presence of the interface dislocations at approximately the spacing calculated is found to occur. In addition to the rearrangement of dislocations near particles, there is a concurrent decrease in the overall average dislocation density (see Table II).

For longer times, the interface dislocations also tend to distort the shape of the γ' particles away from the original rectangular shape. Because of the antiphase domain boundary energy, the single dislocations are prevented from entering the particle, but the line tension of the dislocations wrapped around the particles does give a driving force for distortion of the particles. The particles are thus pinched in where the dislocations encircle them. This effect is shown quite clearly in Fig. 6 where an individual γ' particle is shown in dark-field.

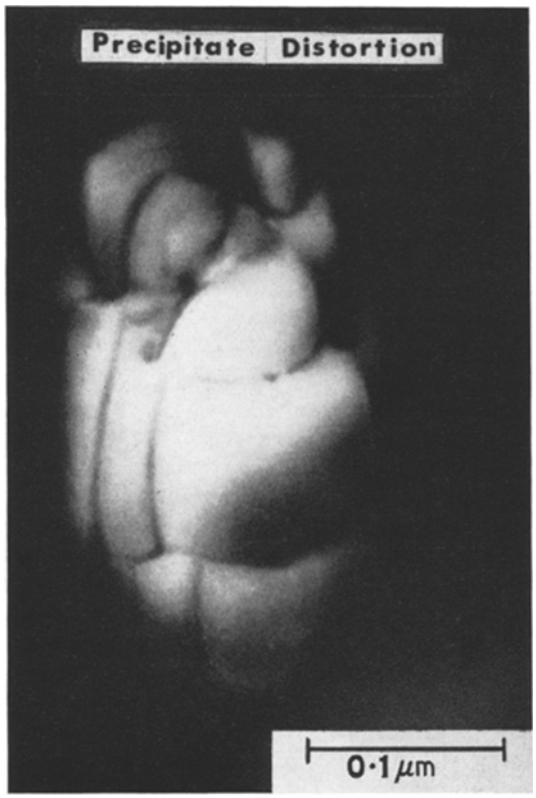

Figure 6 Dark-field superlattice reflection showing distortion of γ' particle by interface dislocations. Alloy LP, 200 h at 735°C, $\epsilon = 10\%$, $t_r = 100$ h at 735°C.

3.2. Precipitate Distribution Effects

Measurements of precipitate size and calculated interparticle spacing for samples of alloy MP aged 200 h at 650, 700 and 735°C are given in Table III along with the yield strength, work-hardening and fractional recovery measurements. The change in γ' distribution affects the recovery measurements and the structural observations. The yield strength is observed to vary inversely with ageing temperature while the amount of work-hardening varies directly. For the lower temperatures of ageing, the deformation is no longer uniform and the 650°C samples have a slip-band deformation structure. The high degree of deformation in the slip bands makes it impossible to observe the condition of the γ' particles within the bands. In the relatively undeformed regions between slip bands, isolated pairs of dislocations could be seen in many cases.

The recovery tests for the three structures were performed at the respective ageing temperatures. Table III also shows that the recovery rates for all three temperatures, based on the recovery parameter, are similar. This is somewhat surprising in view of the 85°C difference in recovery temperatures. The explanation of this effect is not clear although it may be due to the inhomogeneous deformation in the 650 and 700°C samples requiring shorter-distances for the dislocations to climb to positions of annihilation, especially in regions where the slip bands on different slip systems intersect. There is also a considerable area of the samples that does not undergo deformation during straining in the 650 and 700°C samples. This material may be the source of deformation following recovery.

3.3. Strain

Fig. 7 shows the fractional recovery and residual internal hardening with recovery time of alloy SS for strains of 5 and 10% plus the average work-hardening. The 20% strain samples were partially recrystallized at the end of 10 h annealing and completely after 50 h. The 5% strain samples recover less than the 10% samples on both a

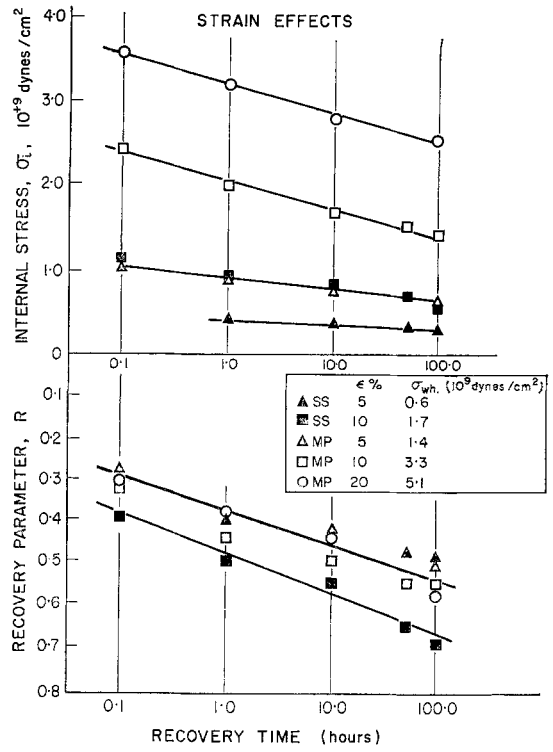

Figure 7 Recovery results for varying prestrain on basis of internal stress and recovery parameter. All samples recovered at 735°C.

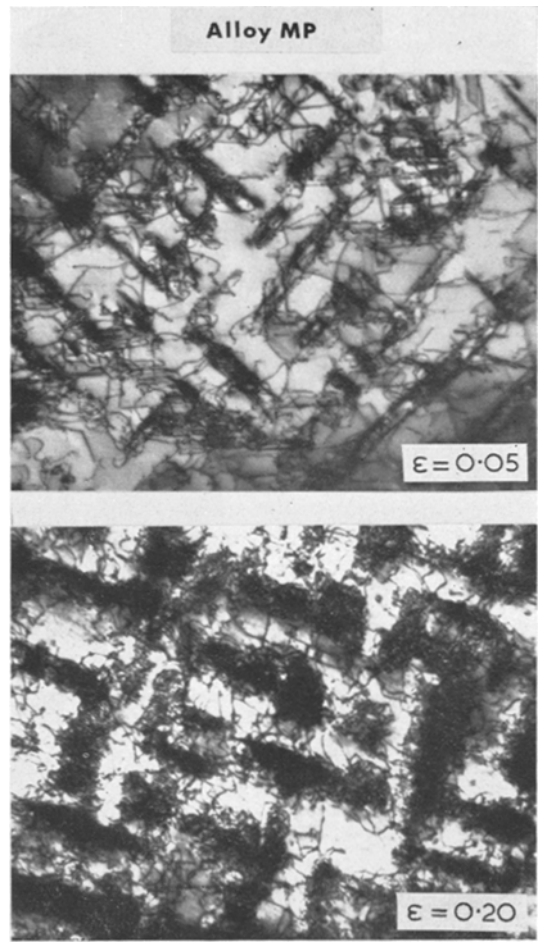

Figure 8 As-deformed substructure for alloy MP prestrained 5 and 20%.

fractional recovery and internal hardening basis.

Fig. 7 also shows the same results for alloy MP. On a fractional basis, there is no measurable difference in the recovery rates for the 5, 10, and 20% strained samples. However, if one considers σ_i, the 10 and 20% strained samples recover at about the same rate which is higher than the 5% samples. The primary difference in structure, as shown in Fig. 8, for the various strains in alloy MP is the density of dislocations between particles. The interparticle density varies as 17, 25, and 30 × 10^9/cm^2 for increasing amounts of strain.

Observation of the dislocation substructure changes accompanying recovery show the interfacial dislocation networks to more nearly approximate the geometry and spacing required to accommodate the lattice mismatch as the prestrain increases. For 5% strain, the networks are not complete with only one or two dislocations at the interface so that complete accommodation of the mismatch is not accomplished. For all strains, the longer time recovery treatments also involve a decrease in the interparticle dislocation density.

3.4. Temperature of Recovery

All tests reported in this section are for samples that were aged at 735°C and then recovered at temperatures below the ageing temperature. The solubility of Al in Ni decreases with decreasing temperature so that the composition of the matrix in alloys LP and MP varies from 12.4 to 11.9 at. % aluminium for temperatures of 735 and 650°C respectively. This makes the quantitative interpretation of results somewhat unclear since any assumption of a constant precipitate structure during the recovery tests is doubtful. Alloy LP samples recovered at temperatures slightly below the ageing temperature showed the precipitation of additional γ' during recovery in the form of a fine dispersion. Alloy MP showed no such secondary precipita-

tion when recovered below the ageing temperature perhaps due to the more closely spaced particles absorbing the additional γ' rather than new precipitates forming although there was no measurable change in average particle size.

For the samples of alloy MP recovered 1 h at various temperatures, there was measurable recovery down to 550°C with recovery parameters of 0.30 for 700°C, 0.15 for 650°C, and 0.06 for 550°C.

A complete series of tests was also run on alloy SS at 650°C to find the temperature dependence of recovery rate for this alloy since the assumption of equivalent structures is more realistic in the single-phase materials. The fractional recovery values are 0.27 for 0.1 h, 0.3 for 1.0 h, 0.35 for 10 h, and 0.4 for 100 h.

4. Discussion

The electron microscopy studies of recovered samples show that the significant feature in the long time ($t > 1$ h) recovery process is a decrease in density of the three-dimensional dislocation network. As proposed by Friedel [10], the rate of flow-stress recovery of a material with a three-dimensional network of dislocations can be related to the rate of growth of the network size (spacing between dislocations). Assuming $\sigma_i = \alpha\mu b\sqrt{\rho}$, a relation of the form

$$\frac{d\sigma_i}{dt} = -\frac{\alpha\mu b}{L^2}\left(\frac{dL}{dt}\right) \tag{4}$$

can be obtained where σ_i is defined as the residual internal hardening, ρ is the dislocation density, L is the spacing between dislocations, α is a geometrical constant and μ and b have their usual meanings. Taking the increase in the spacing of dislocations to be controlled by diffusion-limited climb [22] in response to line tension, we can write the climb velocity [23]

$$V = \frac{dL}{dt} \simeq \frac{Db^3\mu}{kTL} \tag{5}$$

where D is the self-diffusion coefficient.

Combining Equations 4 and 5 and integrating we obtain

$$(1/\sigma_i)^2 = \frac{2Db\,t}{kT\alpha^2\mu} + C \tag{6}$$

where C is an integration constant. If this model is obeyed, then a plot of $(1/\sigma_i)^2$ versus time should give a linear relation with slope proportional to the diffusion coefficient.

Fig. 9 is such a plot for the three alloys and it shows for times greater than 10 h, a linear relation between $(1/\sigma_i)^2$ and time is followed for all three alloys. The shorter times show deviation from linearity for all alloys. For alloy SS, this is probably due to the annealing out of the small loops and debris and the initial rearrangement of the slip band dislocations of the as-deformed state into fine networks. For LP and MP, the mechanism of recovery at short times is probably associated with the annealing of small loops and dipoles plus a contribution due to relaxation of the lattice mismatch strain when the networks of dislocations form at the γ'-matrix interface.

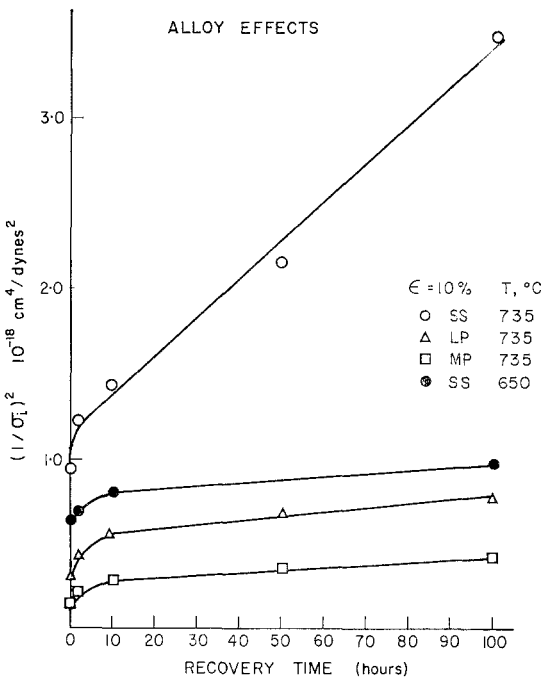

Figure 9 Comparison of recovery results with Friedel model of recovery. All samples prestrained 10%.

If the long-time ($t >$ few hours) recovery data follow Equation 6 then the activation energy for the process should be equal to that for self diffusion. By obtaining the value of the slope from plots such as Fig. 9, for different temperatures, it is possible to obtain a measure of the activation energy for recovery ($t > 10$ h). This was done for the samples of alloy SS that were recovered at 735 and 650°C. An activation energy of 60 ± 10 kcal/mol was obtained which is near the activation energies for diffusion of Ni [24] and Al [25] in Ni (~65 kcal/mol). Activation energies were not obtained for the γ'

strengthened alloys because of the problem of concurrent precipitation when ageing at different temperatures.

As a further test of the validity of Equation 6 the slopes of the curves in Fig. 9 can be compared with the predicted slope. Taking $D = 4 \times 10^{-15}$ cm^2/sec [24], $b = 2.5 \times 10^{-8}$ cm, $\mu = 7 \times 10^{11}$ dyn/cm^{-2}, $kT = 1.4 \times 10^{-13}$ erg (735°C), $\alpha \approx 0.8$, the computed slope is 3.3×10^{-21} cm^4 dyn^{-2} sec^{-1}, whereas the measured slopes are much smaller, e.g., 7.7×10^{-24} cm^2 dyn^{-2} sec^{-1}, for alloy SS. This difference in slope may be a result of dislocations not acting as perfect line sources and sinks of vacancies as demanded from Equation 5. For example, if dislocations climb by point defect emission or absorption at discrete jogs along the dislocation line and these jogs have spacing λ, then to a first approximation Equation 5 can be rewritten

$$V = \frac{Db^4\mu}{kT\lambda L} \tag{7}$$

The difference in calculated and measured rates would set the value of λ at about $100b$ for alloy SS under the conditions investigated. Because of the close correspondence of recovery activation energy and diffusion activation energy it seems unlikely that λ could represent an equilibrium thermal jog spacing. If this were the case the measured recovery activation energy should be the sum of the diffusion and jog-formation energies.

When the change in internal stress is plotted according to Equation 6, allowance is made for the variation in the driving force for recovery due to the varying initial work-hardening. It can be seen that the addition of the γ' considerably reduces the recovery rate, as indicated by a decrease in slope for the precipitation-hardened alloys in Figs. 9 and 10. This decrease in slope can be related to the observation that for alloy MP, the average dislocation segment length for the as-deformed state as calculated from the density measurements is of the order of the interparticle spacing. Therefore, many dislocation segments intersect γ'-matrix interfaces with about the same regularity that they intersect other dislocations. Hence, the net climb force of any dislocation segment can be considerably below the "unimpeded" value used in the derivation of Equation 5. This effectively reduces the rate at which the network of dislocations tends to coarsen and thus reduces the recovery rate. In essence the second phase will stabilize the network size at some finite dimension determined by the precipitate distribution and material parameters [26]. As a result the recovery behaviour of γ'-strengthened alloys would not be expected to obey Equation 6 but should proceed more slowly as the dislocation spacing increases. That is, $(\mathrm{d}\sigma_i)/\mathrm{d}t$ will be given by an expression similar to [27]

$$\frac{\mathrm{d}\sigma_i}{\mathrm{d}t} = \frac{Db^2\sigma_i^2}{\alpha kT}\left(\frac{\sigma_i}{\alpha\mu b} - z\right) \tag{8}$$

where the parameter z represents a retarding force or back-stress due to the presence of the γ' particle. To a first approximation z is about equal to the reciprocal of the particle spacing (assuming non-deformable particles). Thus recovery should cease when $L \sim z$ or $\sigma_i \sim 10^9$ dyn/cm^{-2} for $z \sim 10^5$ cm^{-1}. The data are not inconsistent with this prediction as one might argue that the results for the γ'-strengthened alloys in Fig. 9 show an asymptotic approach to a limiting σ_i value rather than a linear relationship between $1/\sigma_i^2$ and time.

Thus, although Figs. 3 and 7 show a continuous increase in the rate of flow stress recovery $(-[\mathrm{d}\sigma_i]/\mathrm{d}t)$ with increasing σ_i, the relative recovery rate on the basis of a network growth model $([\mathrm{d}(1/\sigma_i)^2]/\mathrm{d}t)$ is decreased by the presence of γ'. This general result was expected from the indirect evidence of the variation in creep-rate for alloys with and without γ' where the presence of the γ' reduces the creep-rate by a factor of 10^3 [21].

Fig. 10 is a plot of $(1/\sigma_i)^2$ versus time for varying amounts of prestrain in alloy SS. As expected from the assumptions of the Friedel model, the results for different prestrains are displaced vertically due to differences in the initial internal hardening, but the slopes are approximately equal. Similar data in Fig. 11 for alloy MP, however, show a considerable difference in slope for the varying amounts of prestrain, the rate of recovery increasing with decreasing prestrain. The Friedel model would again predict the same slope for the differing strains, or if the γ' is taken into account the slope would *decrease* with decreasing prestrain as the dislocation spacing increases relative to the γ' spacing. In presenting the electron microscopy results for varying strain, it was noted that there was a difference in the spacing and perfection of the networks at the γ'-matrix interface for the various strains. The 20% strain samples had the most nearly perfect networks, the more lightly strained samples having interfacial networks with decreasing perfec-

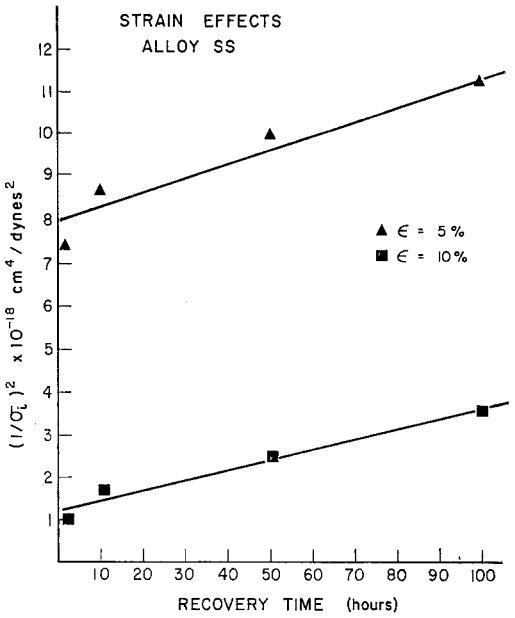

Figure 10 Comparison of prestrain effects in alloy SS with Friedel model. Recovered at 735°C.

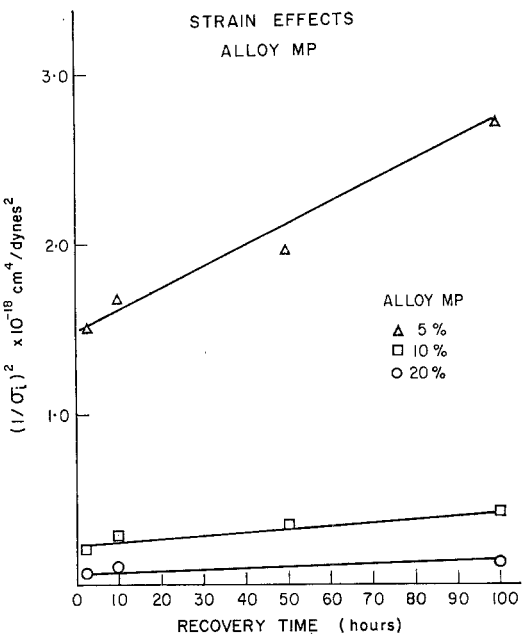

Figure 11 Comparison of prestrain effects in alloy MP with Friedel model. Recovered at 735°C.

tion and a spacing greater than that necessary for complete relaxation of the lattice mismatch. It is possible that the larger slopes in Fig. 11 for the lower strains is due to the attraction of additional dislocations to the matrix-particle interface. That is, the coherency strains in the low-prestrain samples provide an additional driving force for dislocation recovery by attracting interparticle dislocations to the γ'-matrix interface. As these coherency strains are fully accommodated for higher prestrains, the driving force for recovery in these samples is merely the interparticle dislocation density. Correspondingly, it is reasonable to expect the low prestrain samples to recover more rapidly* than samples with larger prestrains even though the interparticle dislocation density increases with prestrain.

An integral part of the above analysis is the assumption that $\sigma_i = \alpha\mu b\sqrt{\rho}$ and this assumption warrants some proof. Fig. 12 is a plot of the

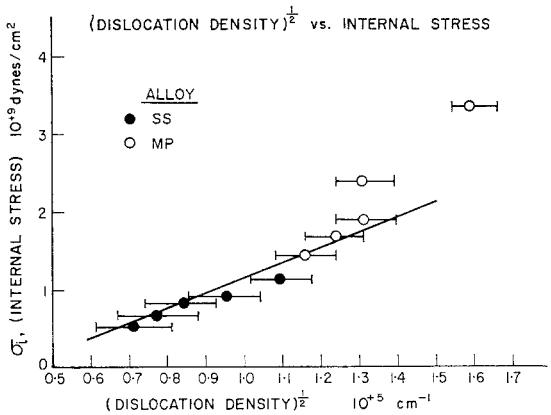

Figure 12 Relation between dislocation density and internal stress for alloys SS and MP. Strained 10% and recovered varying times at 735°C.

dislocation density to the one-half power versus the internal stress for all the samples of alloys SS and MP where dislocation density counts were given in Table II. As can be seen, there is good agreement within the accuracy of the measurements for a linear relation of dislocation density to the one-half power and internal stress for all samples except alloy MP in the as-deformed state and after 0.1 h recovery. The displacement of these two points suggests that the dislocation clustered around the γ' particles contribute to the flow stress and recovery rate for very short times. Only the interparticle dislocations were included in the density measurements and the effective

*The absolute rate of recovery $(-[d\sigma_i]/dt)$ for alloy MP increases with increasing prestrain, but when interpreted in terms of network growth model $[(d(1/\sigma_i)^2)/dt]$ the recovery rate decreases with prestrain.

density would be increased if the dislocation surrounding the γ' particles were included. This correction could eliminate the slope change. Evaluation of the constant α yields a value of 0.8, in reasonable agreement with theory and other experimental observations [28].

5. Conclusions

The essential findings of this study can be summarized as follows:

1. The important parameter in describing the recovery behaviour of cold worked metals is the work hardened component of the flow stress, σ_i. Absolute recovery rates, $-(d\sigma_i)/dt$, generally increase with increasing σ_i.
2. For short times, recovery does not follow the predictions of the network growth model. In the solid solution it is characterized by annealing of dislocation loops and the breakdown of the slip bands into fine networks of dislocations. For precipitation-hardened materials, the initial stages of recovery are characterized by the dissolution of the tangles of dislocations around the particles and the formation of networks at the γ'-matrix interface to accommodate the lattice mismatch plus the annealing out of small loops and other localized dislocation arrays.
3. For longer times, recovery does follow the predictions of the network growth model in the solid solution and the mechanism for recovery is a decrease in the overall density of dislocations by the coarsening of the three-dimensional dislocation network.
4. The activation energy measured for recovery of solid-solution alloys at long times is comparable within the accuracy of the measurements to the measured values of diffusion of Ni and Al in Ni.
5. Varying the amount of prestrain does not effect the recovery rate for solid solution alloy SS (in agreement with the network growth model) but a precipitation-hardened alloy MP exhibits a decrease in recovery rate ($[d(1/\sigma_i)^2]/dt$) with increasing prestrain. This is explained on the basis of saturation of the coherency strain effect for the larger prestrains.

Acknowledgements

This project was supported partially by the Advanced Research Projects Agency through the Center for Materials Research at Stanford University and partially by the Atomic Energy Commission through contract number AT (04-3) 326-PA-17. Appreciation is expressed to the International Nickel Company for supplying the material used in this investigation.

References

1. L. HIMMEL (editor), "Recovery and Recrystallization" (Interscience, New York, 1963).
2. "Creep and Recovery" (American Society for Metals, Cleveland, 1957).
3. R. W. CAHN, Recovery and Recrystallisation, in "Physical Metallurgy" (R. W. Cahn, ed.), 2nd edition (John Wiley, New York, 1970) p. 1129.
4. J. L. LYTTON, K. H. WESTMACOTT, and L. C. POTTER, *Trans. AIME* **233** (1965) 1757.
5. J. E. BAILEY and P. B. HIRSCH, *Phil. Mag.* **5** (1960) 485.
6. L. M. CLAREBROUGH, M. E. HARGREAVES, and M. H. LORETTO, Changes in Internal Energy Associated with Recovery and Recrystallization, in "Recovery and Recrystallization" (L. Himmel, ed.), (Interscience, New York 1963) p. 71.
7. G. C. WEATHERLY and R. B. NICHOLSON, *Phil. Mag.* Ser. 8, **17** (1968) 801.
8. HIROSHI FUMITA, *J. Phys. Soc. Japan*, **26** (1969) 1437.
9. HSUN HU, in "Recovery and Recrystallization" (L. Himmel, ed.), (Interscience, New York, 1963) p. 311.
10. J. FRIEDEL, "Dislocations" (Pergamon Press, Oxford, 1964) p. 277.
11. S. K. MITRA and D. MCLEAN, *Proc. Roy. Soc.* **287** (1966) 288.
12. M. VON HEIMENDAHL and G. THOMAS, *Trans. AIME* **230** (1964) 1521.
13. A. J. ARDELL and R. B. NICHOLSON, *J. Phys. Chem. Solids* **27** (1965) 793.
14. A. TAYLOR and R. W. FLOYD, *J. Inst. Met.* **81** (1952-1953) 451.
15. C. S. SMITH and L. GUTTMAN, *Trans. AIME* **197** (1953) 81.
16. P. BEARDMORE, R. G. DAVIES, and T. L. JOHNSTON (to be published).
17. S. M. COPLEY and B. H. KEAR, *Trans. AIME* **239** (1967) 984.
18. M. B. BEVER, in "Creep and Recovery" (*ASM*, Cleveland, 1957) p. 14.
19. W. GERLACH and W. HARTNAGEL, *Sitzungsberichte der Bayerischen Akademie der Wissenschaften*, München, (1939) 97.
20. G. MASING and J. RAFFELSIEPER, *Z. Metallk.* **41** (1950) 65.
21. F. GAROFALO, "Fundamentals of Creep and Creep Rupture in Metals" (MacMillan, New York, 1965) p. 87.
22. D. N. SEIDMAN and R. W. BALLUFFI, *Phys. Stat. Sol.* **17** (1966) 531.
23. J. P. HIRTH and J. LOTHE, "Theory of Dislocations" (McGraw-Hill, New York, 1968) p. 513.
24. R. A. SWALIN and A. MARTIN, *Trans. AIME* **206** (1956) 567.

25. R. LAGNEBORG, *Met. Sci. J.* **3** (1969) 18.
26. D. MCLEAN, *Trans. Met. Soc. AIME* **242** (1968) 1193.
27. R. LAGNEBORG, *J. Mater. Sci.* **3** (1968) 596.
28. J. D. BAIRD and B. GALE, *Phil. Trans. Roy. Soc.* **257** (1964) 553.

Received 3 January and accepted 26 January 1972.